Journal Pre-proof

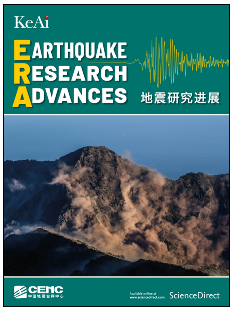

Characteristics of Ambient Seismic Noise Recorded at Offshore Wind Turbine Platform Monitoring Stations

Jun Wang, Jiang-rong Zheng, Ye-jun Sun, Ling-yu Xu, Yi-cheng He, Jie Gong, Chen Wang, Xiao-yan Zhan, Yu-jie Wan, Wen-jie Ren

PII: S2772-4670(25)00083-1

DOI: https://doi.org/10.1016/j.eqrea.2025.100440

Reference: EQREA 100440

To appear in: *Earthquake Research Advances*

Received Date: 3 April 2025

Revised Date: 8 November 2025

Accepted Date: 24 November 2025

Please cite this article as: Wang, J., Zheng, J.-r., Sun, Y.-j., Xu, L.-y., He, Y.-c., Gong, J., Wang, C., Zhan, X.-y., Wan, Y.-j., Ren, W.-j., Characteristics of Ambient Seismic Noise Recorded at Offshore Wind Turbine Platform Monitoring Stations , *Earthquake Research Advances*, https://doi.org/10.1016/j.eqrea.2025.100440.

Characteristics of Ambient Seismic Noise Recorded at Offshore Wind Turbine Platform Monitoring Stations

Jun Wang[1], Jiang-rong Zheng[1],Ye-jun Sun[1], Ling-yu Xu[2], Yi-cheng He[1],

Chen Wang[1], Jie Gong[1], Yu-jie Wan[3], Wen-jie Ren[2]

[1]Professor, Earthquake Administration of Jiangsu Province, Nanjing 210014, China. Email: wangjun1099@qq.com, Phone: 13951702501.

[2]Professorr,Earthquake Administration of Jiangsu Province, Nanjing 210014, China. Email: jsdzjzjr@126.com.

[3]Professorr,Earthquake Administration of Jiangsu Province, Nanjing 210014, China. Email: syj_4116@126.com.

[4] Professorr Institute of Geotechnical Engineering, Nanjing Tech University, Nanjing 210009, China. Email: lyxu@njtech.edu.cn

[5]Associate professor,, Earthquake Administration of Jiangsu Province, Nanjing 210014, China. Email: hyckevin@mail.ustc.edu.cn

[6]Engineer, Earthquake Administration of Jiangsu Province, Nanjing 210014, China. Email:372766770@qq.com

[7]Associate professor, Earthquake Administration of Jiangsu Province, Nanjing 210014, China. Email: 498602259@qq.com

[8]Engineer, Earthquake Administration of Qinghai Province, Xining 810000, China。 Email:376633212@qq.com

[9]PhD candidate, Institute of Geotechnical Engineering, Nanjing Tech University, Nanjing 210009, China. Email:renwenjie@njtech.edu.cn

Corresponding author: Jun Wang, wangjun1099@qq.com

Characteristics of Ambient Seismic Noise Recorded at Offshore Wind Turbine Platform Monitoring Stations

Abstract: This study examines ambient seismic noise recorded from operational seismic monitoring stations installed on offshore wind platforms in the Yellow Sea. The research utilizes one-year three-component continuous waveform data to investigate energy intensity, wavefield composition, and polarization properties through frequency-domain polarization analysis. A dynamic finite element analysis is conducted on a typical offshore platform structure to investigate the amplification effect. The results show that: (1) The energy of single-frequency microseisms is clearly observable, while distinct segmentation phenomena are observed near 0.2 Hz within the double-frequency microseism (DF) band, with short-period DF exhibiting stronger energy than long-period DF. The wind, wave and current may result in greater horizontal noise energy intensity than vertical components at specific frequencies and directions; (2) The ambient seismic noise recorded at offshore platform monitoring stations exhibits systematic amplification compared to onshore station observations, with an average amplification factor of 3-5 across the studied frequency band. Notably, maximum amplification reaches 6.6-7.7 times within the 1.2-1.6 Hz range, representing a significant resonant response characteristic of the offshore platform structures. (3) Within the microseismic band (20 s-0.5 Hz), the azimuth of the noise polarization principal axis predominantly clusters around 200°. The polarization degree exhibits perturbed variations with frequency between 0.2-0.6 Hz and is slightly greater than that obtained from onshore stations. These observations indicate that hurricane/storm activities and short-period ocean waves in the relevant maritime area, along with their breaking and turbulent processes, generate pronounced high-frequency noise components.

Keywords: Marine seismic observation; Offshore wind power platform; Ambient seismic noise; Frequency-domain polarization analysis; Finite element modeling

1. Introduction

Seismic monitoring provides a basis for understanding earthquake preparation and occurrence mechanisms, investigating the Earth's internal structure, and implementing earthquake early warning systems. However, the current seismic monitoring relies on land-based seismic networks due to the challenges posed by the ocean environment, resulting in a sparse distribution of marine seismic observation stations. This limitation is particularly alarming given that oceans cover approximately 71% of the Earth's surface and marine earthquakes account for about 85% of global seismic activity, as evidenced by global seismic data. With the rapid development of the marine economy, the need for marine seismic observations and the mitigation of marine seismic hazards has become increasingly urgent (Chen et al., 2025; Xu et al., 2025b). Consequently, since the 1960s, many countries have initiated marine seismic observation efforts, progressively advancing research in this field and contributing significantly to marine seismic monitoring, marine seismic structure surveys, and investigation of secondary marine disasters (Stephen, 2003).

With the advancement of science and technology, seismologists have been continuously striving to apply various advanced seismic observation technologies, such as ocean-bottom seismometers (OBS), cabled systems, buoy-based systems, and distributed fiber-optic sensing (DAS), to marine seismic monitoring. However, significant challenges in power supply, data communication, and long-term maintenance, preventing the implementation of sustained, continuous, and fixed seismic observations. These limitations have severely hindered substantial progress in marine seismic observation and its applied research. Thus, most research remain focused on technical validations and short-term seismic recordings. For example, Ito et al. (2017) conducted a one-year observation of volcanic activity in the Pacific using OBS to investigate the earthquake localization and velocity structure. Lin et al. (2024) captured global seismic data during a 3- to 6-month deployment of broadband OBS, including the 7.8 magnitude earthquake in New Zealand and the 6.3 magnitude nuclear test in North Korea. Krylov et al. (2021) reported the effectiveness of broadband Molecular Electronic Transfer (MET) sensors in OBS for high-quality seismic data under Arctic conditions, highlighting their potential use for seismic hazard assessments in Arctic region. In addition, the Earthquake Research Institute of the University of Tokyo has deployed a submarine earthquake and tsunami observation cable system using optical fiber for data transmission in the Sanriku region since 1996. This system has recorded small seismic events of around magnitude 1.8 near the submarine cable and a distant earthquake of magnitude 6.6 with an epicenter approximately 2,300 kilometers away (Shinohara et al., 2022). Baba et al. (2024) conducted marine seismic observation by deploying Distributed Acoustic Sensing (DAS) in the Tsugaru Strait and detected earthquakes with magnitudes below 1.0 during a four-month observation period.

In recent years, the rapid growth of the offshore wind power (OWP) industry has provided new opportunities for marine seismic observation due to the increasing global demand for renewable energy. OWP platforms offer a promising foundation for constructing seismic monitoring stations because they are widely distributed and offer unique advantages in power supply and communication. Since December 2022, the Earthquake Administration of Jiangsu Province (EAJ) of China has progressively established seismic monitoring stations on the OWP platforms (Sun et al., 2022; Zhu et al., 2023) and successfully recorded the dynamic response of the OWP platforms under earthquakes in the Yellow Sea region. In September 2023, the China Earthquake Administration released a document titled "China Marine Seismic Observation Plan (2023-2035)", explicitly proposing the construction of seismic monitoring stations on OWP platforms. Consequently, it is anticipated that more seismic monitoring stations will be deployed in the future. As an effective approach to marine seismic observation, the extraction of spectral characteristics from recorded data and their subsequent application to seismic research and earthquake early warning systems in maritime regions constitute critical scientific questions in the field of seismic monitoring. A comprehensive analysis of ambient seismic noise in continuous recordings from offshore platform monitoring stations offers valuable insights for assessing data quality and utility.

In seismological research, microseism is defined as the most energetic component of ambient seismic noise within the 2-20 second period band. This band exhibits two distinct spectral peaks, classified as single-frequency (SF) microseisms and double-frequency (DF) microseisms, each generated by different excitation mechanisms (Miche, 1944; Hasselmann, 1963; Bromirski et al., 2005; Tanimoto & Prindle, 2007; Koper & Burlacu, 2015; Xiao et al., 2018; Wang Jun et al., 2022). Thus, this study examines continuous waveform data recorded by EAJ between May 2023 and December 2024. The analytical framework incorporates two advanced methodologies: (1) frequency-domain polarization analysis and (2) dynamic response analysis of OWP platforms. This study systematically investigates three fundamental aspects of microseismic phenomena: (1) the source characteristics and underlying generation mechanisms of microseismic noise, (2) the spectral properties of ambient seismic noise, and (3) the potential influence of offshore platform structures on microseismic noise. The results provide critical foundations for developing noise seismology applications and optimizing the use of offshore monitoring station data in seismic research.

2. Offshore platform monitoring stations

Over the years, marine seismic observation has faced persistent operational limitations due to power supply constraints, unreliable communications, and maintenance difficulties, preventing sustained, high-quality seismic monitoring. The integration of seismic monitoring stations with offshore wind platforms now offers a viable solution to these challenges. These installations deploy broadband seismometers that serve three critical functions: (1) enhancing earthquake detection and early warning precision, (2) facilitating high-resolution imaging of marine crustal structures, and (3) enabling structural health monitoring of offshore installations. The EAJ has established seven seismic monitoring stations in the Yellow Sea area, utilizing offshore wind power substations and high-resistance stations as deployment platforms. The distribution of these offshore platforms is listed in Fig. 1. Each monitoring substation is equipped with broadband seismometers and accelerometers, strategically positioned near the primary support columns on the first floor of the platforms, as shown in Fig. 2. The instruments are sealed and protected using an RH-S700 protective housing. The observation data are transmitted in real-time to the data center of the EAJ via a submarine communication system (Gong et al., 2023). Table 1 provides detailed information regarding the platform dimensions, offshore distances, instrument models, and seawater depths for each monitoring substation.

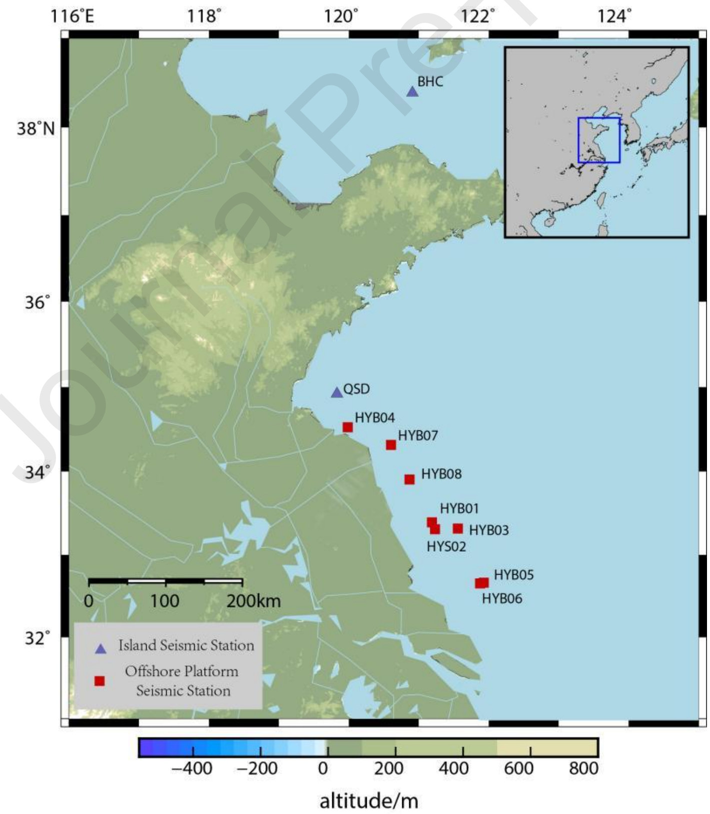

Fig. 1 Distribution of seven seismic monitoring stations on offshore wind power high-voltage substations and step-up substations

Fig. 2 Offshore wind power platform and seismic monitoring devices: (a) Offshore wind substation (red rectangle indicates the installation position for monitoring devices) and (b) A photo showing the installation position of monitoring devices

Table 1 Detailed information of seven monitoring substation.

No.	Name of Substations	Station Code	Equipment	Distance from Shore (km)	Platform Dimensions
1	Dafeng Phase I Step-Up Substation H11	HYB01	GL-PCS60	45	36.50m × 42.00m, 4 floors, height 22m
2	Dafeng Phase II High-resistance Substation H8-2	HYS02	GL-PS2	51	47m × 29.8m, 4 floors, weight approx. 2800 tons
3	Xiangshui Step-Up Substation	HYB04	GL-PCS60	10	25m × 28m, height approx. 25m, 4 floors, total weight approx. 2000 tons
4	Rudong Step-Up Substation H6	HYB05	GL-PCS60	60	39.8m × 43.5m, height 16m
5	Rudong Step-Up Substation H10	HYB06	GL-PCS60	60	39.8m × 43.5m, height 16m, 3 floors
6	Binhai Step-Up Substation H3	HYB07	GL-PCS60	36	38.1m × 41.54m, height 20.9m, 5 floors, weight approx. 3030 tons
7	Sheyang Step-Up Substation H2	HYB08	GL-PCS60	45	56m× 50m, height 29m, weight 3850 tons

Table 2 Detailed parameters of two equipment used for marine seismic observation

Serial Number	Equipment	Seismometer Sensitivity	Data Logger Conversion Factor	Sampling Rate	Frequency Bandwidth
1	GL-PCS60	1000 V/m/s	74.5nV/count	100Hz	60s-50Hz
2	GL-PS2	1000 V/m/s	74.5nV/count	100Hz	2s-50Hz

3. Analysis Procedure

3.1 Polarization Analysis

Polarization analysis is a classic and highly effective technique for extracting kinematic features and characteristics from different components of particle motion (Jurkevics, 1988). It can be classified into two main approaches: time-domain algorithms (Flinn, 1965; Lin et al., 2012) and frequency-domain algorithms (Park et al., 1987; Chen et al., 2007). This study employs a frequency-domain polarization algorithm, which offers the advantage of using prolate spheroidal wave functions for tapering when directly obtaining the signal spectrum, thereby preserving the integrity of the cross-spectral matrix with minimal distortion. The theoretical foundation of this method has been well-documented (Samson, 1983; Park et al., 1987) and will not be elaborated here. The processing of single-station data follows established methodologies (Wang et al., 2020; Wang et al., 2022). Our proposed method assumes that Rayleigh waves are incident as plane waves on each seismic station (Fig. 3). The three-component continuous waveform data are processed using 1-hour segments as computational samples, with a 50% overlap ratio applied to the sliding windows of the 3×3 complex spectral covariance matrices. The spectral estimation employs 10 tapered sub-windows, each with a duration of 819.2 seconds, yielding effective frequency results in the range of 0.016-10 Hz. Prior to computation, the raw data undergoes necessary preprocessing including resampling to 20 Hz and removal of instrument responses.

The polarization analysis extracts the four key parameters:

(1) Power of the polarization corresponding to the largest eigenvalue (λ_0): This represents the power of the principal polarization derived from the analysis of the original three components, expressed in units of acceleration power spectral density (dB, 10*log10(m^2/s^4/Hz)) (Jepsen and Kennett, 1990; Wagner and Owens, 1996). These three components are the vertical (UD), north-south (NS), and east-west (EW) directions. It is a function of azimuth and effectively characterizes the vibrational energy of the signal. Regardless of how the signal is polarized or divided among the three components, its amplitude can be accurately captured across the entire frequency range.

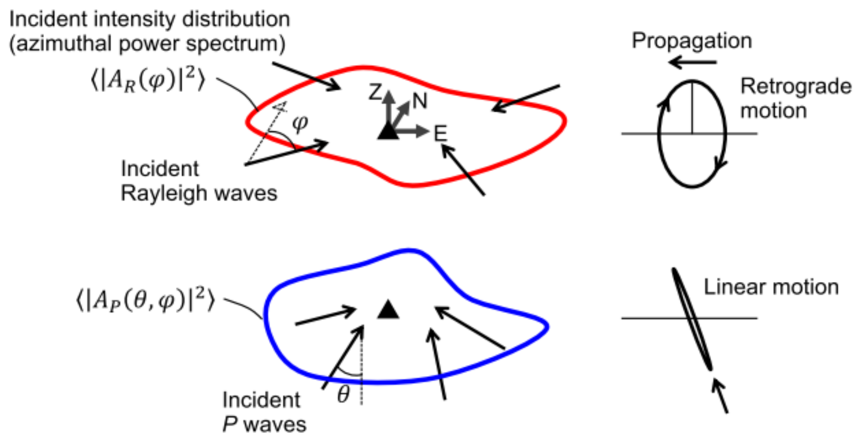

Fig. 3 Schematic illustration of Rayleigh waves and P waves incident on a single three-component station, and particle motions of fundamental-mode Rayleigh (R)and P waves. Black arrows indicate incident Rayleigh and P

waves. φ and θ are propagation azimuth and incident angle. (Takagi et al., 2018)

(2) Degree of polarization (β^2): This parameter is given in Eq. (1):

$$\beta^2 = \frac{nTrS^2 - (TrS)^2}{(n-1)(TrS)^2} \quad (1)$$

where S is the spectral density matrix, n is the length of the data sequence, Tr is the minimization factor under non-negative constraints. β^2 characterizes the degree of signal structure and is a dimensionless quantity representing the correlation between the components of the vibration vector. β^2 ranges between 0 and 1: $\beta^2 = 0$ when all eigenvalues are equal and $\beta^2 = 1$ when only one non-zero eigenvalue exists. For further details, refer to Eq. (31) in Samson (1983).

(3) Polarization ellipse azimuth (θ_H): This parameter represents the azimuth of the major axis of the polarization ellipse, ranging from 0° to 360°. It reflects the back-azimuth of wave sources such as Rayleigh waves or P-waves. Additionally, θ_V represents the incidence angle of P-waves.

(4) Phase difference between radial and vertical components (φ_{VR}): This parameter ranges from -90° to 90°. There exists an equivalence effect between θ_H and φ_{VR} (Koper and Burlacu, 2015). For example, a retrograde Rayleigh wave (φ_{VR} = -90°) arriving from a specific back-azimuth (θ_H = 45°) can be equivalently described as a prograde Rayleigh wave (φ_{VR} = 90°) arriving from the opposite direction (θ_H = 225°).

3.2 Finite element modeling

To analyze the correlation between microseisms and platform structure response, this study uses the implicit dynamics module of the ABAQUS finite element software to develop a mechanical model of the offshore jacket platform. The governing equation for the implicit dynamics analysis module is:

$$\boldsymbol{M}\ddot{\boldsymbol{u}} + \boldsymbol{C}\dot{\boldsymbol{u}} + \boldsymbol{K}\boldsymbol{u} = \boldsymbol{F} \quad (2)$$

where **M** represents the mass matrix，**C** is the damping matrix，**K** denotes the stiffness matrix，**F** is the external force vector, **u,** $\dot{\boldsymbol{u}}$ and $\ddot{\boldsymbol{u}}$ correspond to the displacement, velocity, and acceleration vectors, respectively.

In the dynamic analysis, Rayleigh damping is applied to the entire structure and is defined as:

$$\boldsymbol{C} = \alpha\boldsymbol{M} + \beta\boldsymbol{K} \quad (3)$$

where α and β are the mass and stiffness coefficients, respectively, determined using the first and second natural frequencies of the structure. The Rayleigh damping ratio for the offshore jacket platform is set to 5% in addition a 2% for hydrodynamic damping and 3% for structural damping (Ajamy et al., 2018; Xu et al., 2025a).

To account for fluid-structure interaction during seismic events, the added mass method is employed. The effective mass (m_e) of the structure submerged in seawater is calculated as the sum of the physical mass (m_p) and the added mass (m_a):

$$m_e = m_p + m_a \tag{4}$$

$$m_a = C_a \rho_w A_p \tag{5}$$

where A_p is the cross-sectional area of the structural member, ρ_w is the density of seawater (taken as 1030 kg/m³), and C_a is the added mass coefficient and is set to 1.0 according to DNV-RP-C205. Consequently, the effective density of the steel structural members submerged in seawater is determined to be 8880 kg/m³ (Xu et al., 2025c).

4. Results and Discussions

4.1 Characteristics of microseismic noise power

The polarization magnitudes obtained within individual weak-polarization noise sub-windows are not entirely stable (Koper and Hawley, 2010). In addition, low-probability transient signals such as seismic events, system calibrations, and environmental disturbances can also influence the characteristics of microseismic noise derived from continuous recording data. Therefore, to capture the non-random properties of the noise field at a substation, it is necessary to analyze a large number of measurements over sufficiently long time to yield practically meaningful results. Moreover, to mitigate the effect of random signals on the inherent microseismic noise characteristics of the substation, we use a probability density function (PDF) approach by extracting the maximum probability distribution curve to represent the station's intrinsic microseismic noise characteristics.

Fig. 4 shows the power (λ_0) of microseismic noise at four offshore platform monitoring stations. The noise power at the stations generally exceeds that observed from Peterson's (1993) High Noise Model (NHNM) across the entire frequency range. The average noise power within the 1~20 Hz frequency range is approximately -91 dB and is higher than the Class V ambient noise power typically observed at land-based stations. A distinct peak is observed between 1-2 Hz, likely attributed to the resonance effects of the platform structure. Within the microseismic frequency band, the energy of single-frequency (SF) microseisms is clearly visible, while the double-frequency (DF) band exhibits a segmentation phenomenon near 0.2 Hz. The spectral power is predominant in the frequency ranges of approximately 0.1~0.25 Hz and 0.25~1.0 Hz, with peaks occurring near 0.2 Hz (5 s) and 0.4 Hz (2.5 s), respectively.

To further elucidate the noise characteristics observed at offshore platform stations, Fig. 5 presents the noise power spectra from two island-based stations. These two stations are the Beihuangcheng Island Station (BHC), located in the Bohai Strait, and the Qiansandao Station (QSD), situated in the sea area of Lianyungang, Jiangsu Province. Both stations are approximately 40 km from the nearest landmass, with their observation equipment deployed on bedrock. The locations of these two stations are also illustrated in Fig. 1. The noise characteristics in Fig. 5 are similar to those observed at island stations in comparable environments. The results demonstrate that the continuous seismic data recorded at offshore platform stations effectively capture the microseismic noise characteristics of island-based stations. This finding underscores the capability of offshore platforms to provide reliable and representative noise data, consistent with observations from nearby island stations.

Moreover, according to the previous studies (Bromirski et al., 2005; Sun et al., 2013; Koper and Burlacu, 2015), DF microseisms are classified into long-period double-frequency (LPDF) and short-period double-frequency (SPDF) microseisms, with the energy of SPDF being stronger than that of LPDF. Bromirski et al. (2013) suggested that near-coastal reflections are the primary source for microseismic noise above 0.12 Hz, primarily generated by wave interactions involving gravity waves with periods of approximately 18 seconds (wavelengths of approximately 500 m) or shorter. Spectral peaks above 0.2 Hz are attributed to a relatively large source region formed by the interaction of shorter-period monsoon-forced waves near the station. The wave period in the Yellow Sea ranges between 3-3.4 seconds, which theoretically can generate a frequency spectrum above 0.2 Hz. This explains why distinct segmentation phenomena are clearly observed near 0.2 Hz within the DF frequency band range (see Fig. 4).

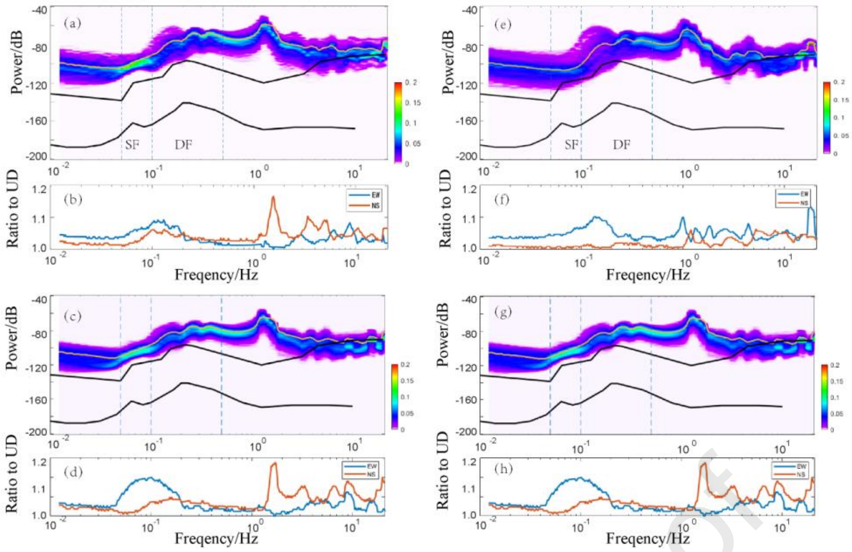

Fig. 4 Polarization analysis from four offshore platform monitoring stations: the power of ambient seismic noise for (a) HYB05, (c) HYB06, (e) HYB07, and (g) HYS02; the ratio of the maximum horizontal power to the maximum vertical power for (b) HYB05, (d) HYB06, (f) HYB07, and (h) HYS02

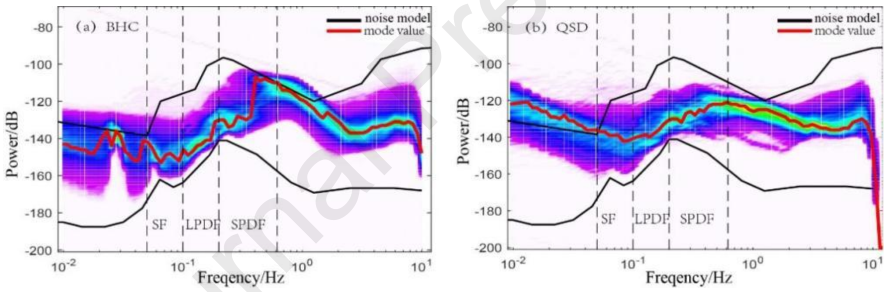

Fig. 5 The power of ambient seismic noise at island-based stations: (a) BHC and (b) QSD

By comparing Fig. 4 and 5, it is evident that the noise power at the offshore platform monitoring stations exhibit an overall structural amplification effect compared to those of the island-based stations. In addition, the ratio of the maximum horizontal power to the maximum vertical power consistently exceeds 1 across all frequencies (Fig. 4b, 4d, 4f, and 4h). This indicates that the amplification effect of microseismic noise energy is stronger in the two horizontal components than in the vertical component. A peak amplification effect with a normal distribution shape is observed in the low-frequency range near 0.1 Hz, while the amplification fluctuates in the high-frequency range above 1 Hz and is strongest near 1.5 Hz.

Fig. 4b also shows that the amplification effect in the NS component is stronger than that in the EW component at the HYB05 station. In contrast, the amplification effect in the EW component is stronger than that in the NS component at the HYB07 station (Fig. 4f). The amplification effect of ambient seismic noise is more pronounced in the EW component at approximately 0.1 Hz for both HYB06 and HYS02 stations. This is because of specific environmental factors such as hydrology, sea conditions, wind, and waves at the platform locations, which can enhance noise energy at specific frequencies and directions (Webb, 1998; Tsai, 2011).

In the Yellow Sea, the sea waves are predominantly wind-generated waves, with the effective wave height being significantly greater than that of swell. Moreover, northward waves account for 55% of the total wave frequency. In the northern Yellow Sea, northwest waves rank second in frequency, while in the central and southern Yellow Sea, north-northeast waves are secondary, both with frequencies ranging from 20% to 25% (Chen et al., 2016). According to data from the National Marine Environmental Forecasting Center, the average wave direction in the Yellow Sea between January 2024 and December 2024 is plotted in Fig. 6. Overall, the wave direction in the area of station HBY05 is predominantly EW direction, with the maximum microseismic noise power in the NS direction being stronger than that in the EW direction. The microseismic noise observed from the HYB07 station exhibits similar characteristics, with waves approaching a NS direction, but the maximum microseismic noise power in the EW direction surpasses that in the NS direction. In other words, waves amplify microseismic noise power perpendicular to their propagation direction.

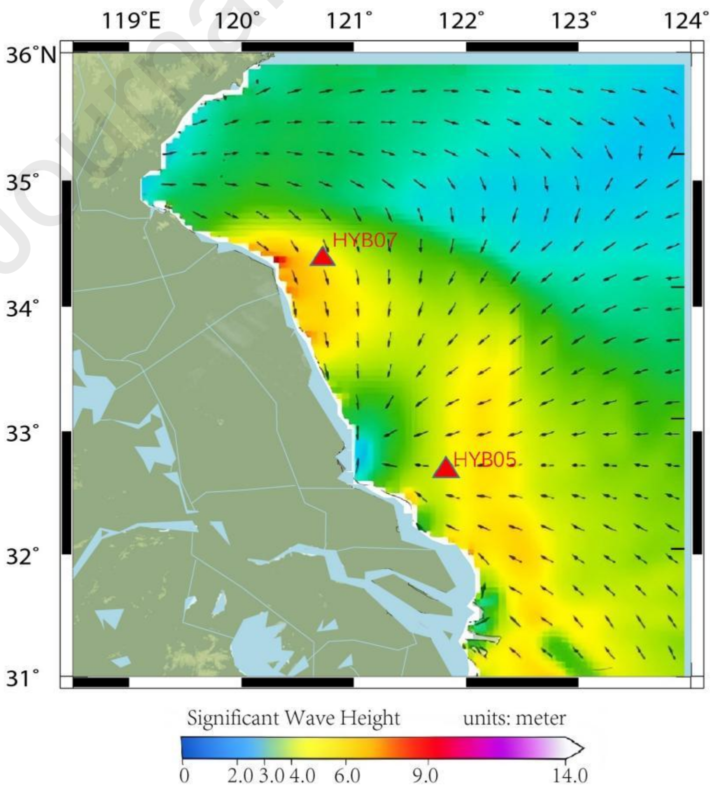

Fig. 6 Wave direction distribution in the Yellow Sea area between January 2024 and December 2024

4.2 Correlation between microseisms and platform structure response

As discussed in Section 3.1, the ambient seismic noise recorded at the offshore platform monitoring stations demonstrates a general amplification effect compared to that from the land-based stations for two primary reasons: (1) The amplitude of the Earth's ambient seismic noise significantly amplifies as it propagates through the seabed mudline to the first floor of the offshore platform, covering a distance of 26.5 m. According to the Chinese GB 50011-2010 and the American ASCE 7 standards, the ratio of the peak floor acceleration of steel structures to the base input peak acceleration (i.e., the peak floor amplification ratio) can reach up to 3. Research by Zou et al. (2023) indicates the floor amplification factor of steel structures may even exceed 5; (2) The offshore wind power platform structure generates dynamic responses under the action of waves, wind, and other environmental factors, increasing the likelihood of resonance and subsequently amplifying the surrounding seismic noise.

The observations demonstrate that recorded data from offshore platform monitoring stations exhibit significant amplification effects, which are closely related to the structural modal characteristics. This study conducted structural modal analysis and dynamic response analysis of a typical offshore platform to quantitatively investigate the amplification effects. This can provide a scientific basis for properly utilizing platform monitoring station data for earthquake rapid reporting, earthquake early warning, and noise seismology studies. To further quantify the amplification factor of the offshore structure on the ambient seismic noise, this study performed finite element analysis of the dynamic structural response under various frequency excitations. We chose a typical monitored platform (i.e., HYS02) for seismic response analysis, which is composed of an upper four-floor platform, a lower jacket foundation, and 4 steel pipe piles (see Fig. 7). The platform's beams are primarily made up of I-beams. In finite element analysis, the substation structure is modeled using beam elements (B31), with materials adopting an ideal elastic-plastic constitutive model. Fig. 7 also shows that the structure mainly utilizes two types of materials: Q355C for the orange components and DH36 for the blue components, with specific parameters detailed in Table 2.

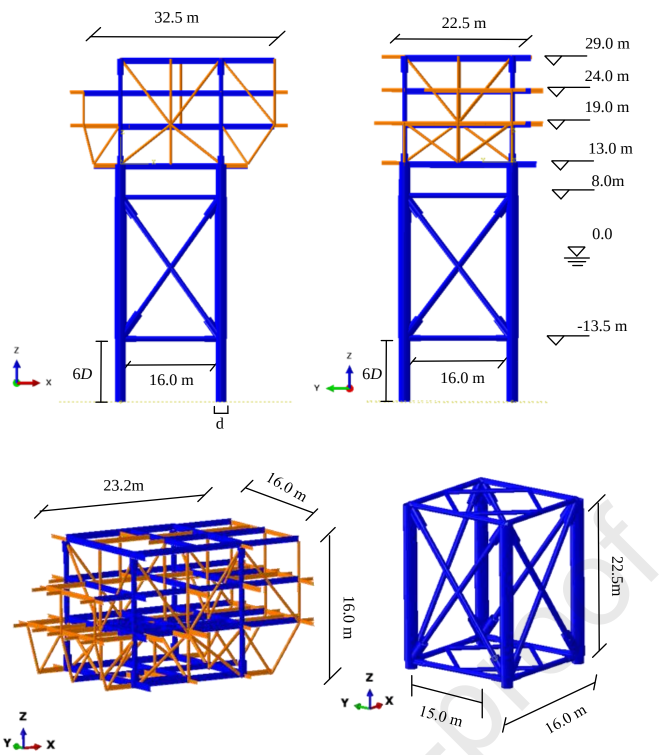

Fig. 7 Finite element modeling of the monitored HYS0 substation structure

Table 2 Material parameters

Material type	Density (kg/m³)	Elastic parameter		Plastic parameter
		Yong's Modulus (Pa)	Poisson's Ratio	Yield Stress（Pa）
DH36	7850	2.1×10^{11}	0.3	3×10^{8}
Q355C	7850	2.06×10^{11}	0.3	3.55×10^{8}

To account for the effect of pile-soil interaction on the upper structure, the numerical model is fixed at a location 6 times the pile diameter below the base of the jacket (Ye and Xin, 2024), and modal analysis is carried out on the offshore structure. Table 3 gives the first 5 modes of the offshore structure.

Table 3 First 5 modes of the monitored HYS0 offshore substation structure

Mode	Number Frequency (Hz)	Circular Frequency (rad/s)
1	1.1991	7.534168
2	1.459	9.167167
3	1.5903	9.99215
4	1.8402	11.56232
5	2.4311	15.27505

In the dynamic analysis, a sinusoidal acceleration excitation with an amplitude of 1 m/s is introduced at the fixed base. Fig. 8 shows the relationship between the peak floor amplification ratio and the frequency of input sinusoidal waves at four floors of the substation structure. The results show that the peak floor amplification ratios exhibit a similar pattern with the input frequency across different floors and generally increase with the floor's height. As a results, the peak floor amplification ratios peak at the top floor. Notably, the peak floor amplification ratios peaks between 1.2 Hz and 1.6 Hz with corresponding values ranging from 6.6 to 7.7. This can be attributed to the excitation frequency being close to the first three modal frequencies of the offshore structure, thereby causing the resonance of the structure. This can support the observed peak amplitudes in the intensity of ambient seismic noise within the range of 1~2 Hz shown in Fig. 4a, 4c, 4e, and 4g.

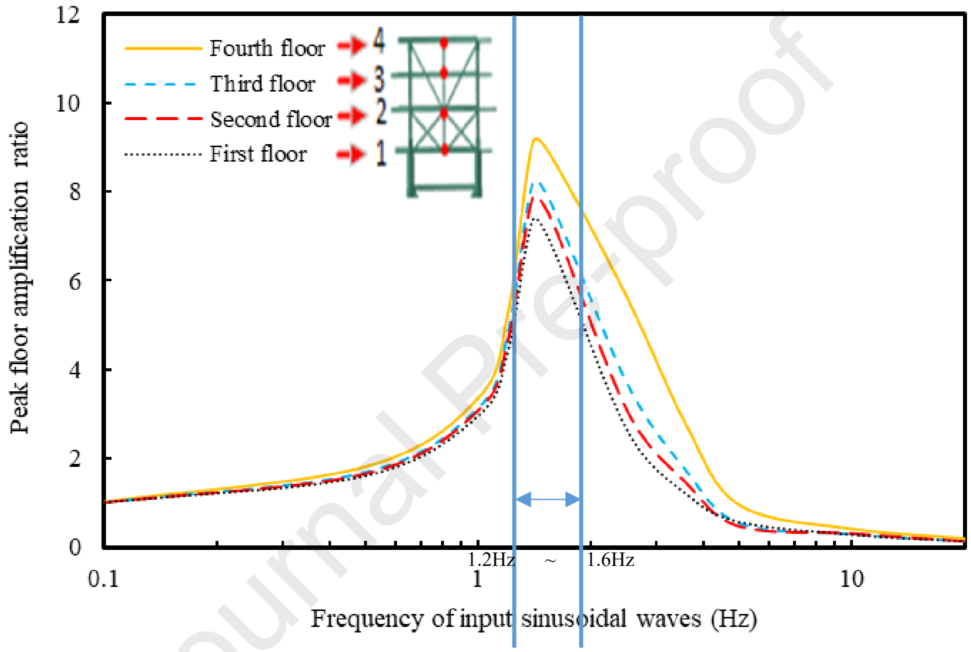

Fig. 8 Relationship between the peak floor amplification ratio and the frequency of input sinusoidal waves at four floors of the substation structure.

4.3 Analysis of Microseismic Polarization Characteristics

To further analyze the characteristics of microseismic noise at the offshore platform monitoring stations, Fig. 9a and 9e present the θ_H obtained from the noise polarization analysis. It can be observed that the azimuth of the primary polarization axis is predominantly concentrated around 200° within the microseismic frequency band. This is consistent with the findings of Wang et al. (2022), who reported that the polarization azimuths of most stations in eastern China are mainly distributed between 160° and 240°. This suggests that the noise sources recorded at the offshore platform stations are similar to those observed at land-based stations, with the dominant polarization direction projected along a great-circle path pointing toward the Indian Ocean in the southwest (Wang et al., 2022). For noise signals above 1 Hz, the polarization directions exhibit higher clustering across the entire frequency range. The θ_H at the HYB05 station shows a primary distribution along 30° to 200°, while the θ_H at the HYB07 station varies between 150° and 350°. The high-frequency signals primarily originate from near-field noise sources, which may be associated with the inherent vibration sources of offshore wind turbine platform facilities. The variation in signal directionality correlates with the relative installation positions of the monitoring equipment on the platform.

For the low-frequency band below 0.05 Hz, the β^2 exhibits a scattered distribution ranging from 0.2 to 0.8 (see Fig. 9b and 9f). This indicates that the SF microseisms show insignificant kinematic differences between vertical and tangential motions. The dominant eigenvector does not represent pure Rayleigh waves but likely a mixture of Rayleigh waves, Love waves, and body waves, consistent with observations from land-based stations in low-frequency ranges (Koper and Burlacu, 2015). Moreover, a distinct and pronounced peak of approximately 0.9 near 0.1 Hz is observed within the microseismic frequency band. This is followed by a decrease to approximately 0.2 as the frequency increases toward 0.2 Hz. Correspondingly, the θ_V exhibits clear segmentation characteristics at 0.1 Hz, with relatively broad θ_V distributions observed around this frequency (see Fig. 9c and 9g).

Fig. 9d and 9h shows that the φ_{VR} probability is widely distributed in the microseismic band, further suggesting weak vertical motion. However, the θ_V probability on both sides peak sharply near 90° (see Fig. 9c and 9g). The results indicate that horizontal motion predominates over vertical motion in both the 12-20s and 2-10s frequency bands. This implies a notable platform resonance effect at 0.1 Hz that amplifies vertical microseismic signals.

For frequencies above 1 Hz, the β^2 fluctuates with increasing frequency for both offshore stations and maintains intermediate levels between 0.3 and 0.6. In contrast, land-based stations typically show lower polarization degrees ($\beta^2 < 0.2$) in this high-frequency band. This indicates that stronger polarization can be observed in offshore platform recordings at certain frequencies, especially revealing significant differences in high-frequency wavefield characteristics between marine and terrestrial stations. These differences are likely due to short-period waves generated by wind-wave interactions in the sea, where wave breaking and turbulent processes can generate high-frequency noise.

The corresponding vertical-radial phase difference (φ_{VR}) follows a near-zero degree distribution, indicating synchronous propagation of vertical and radial components of seismic wave with zero phase difference between two components. This phenomenon typically occurs during compressional (P-) wave propagation, where the vibration direction aligns with the propagation direction, representing simple and symmetric wave modes. Such observations may also suggest either homogeneous medium properties or relatively simple wave propagation paths. Moreover, for frequencies above 1 Hz, approximately zero φ_{VR} implies simple wave propagation patterns, with geometric configurations or polarization states exhibiting high degrees of symmetry.

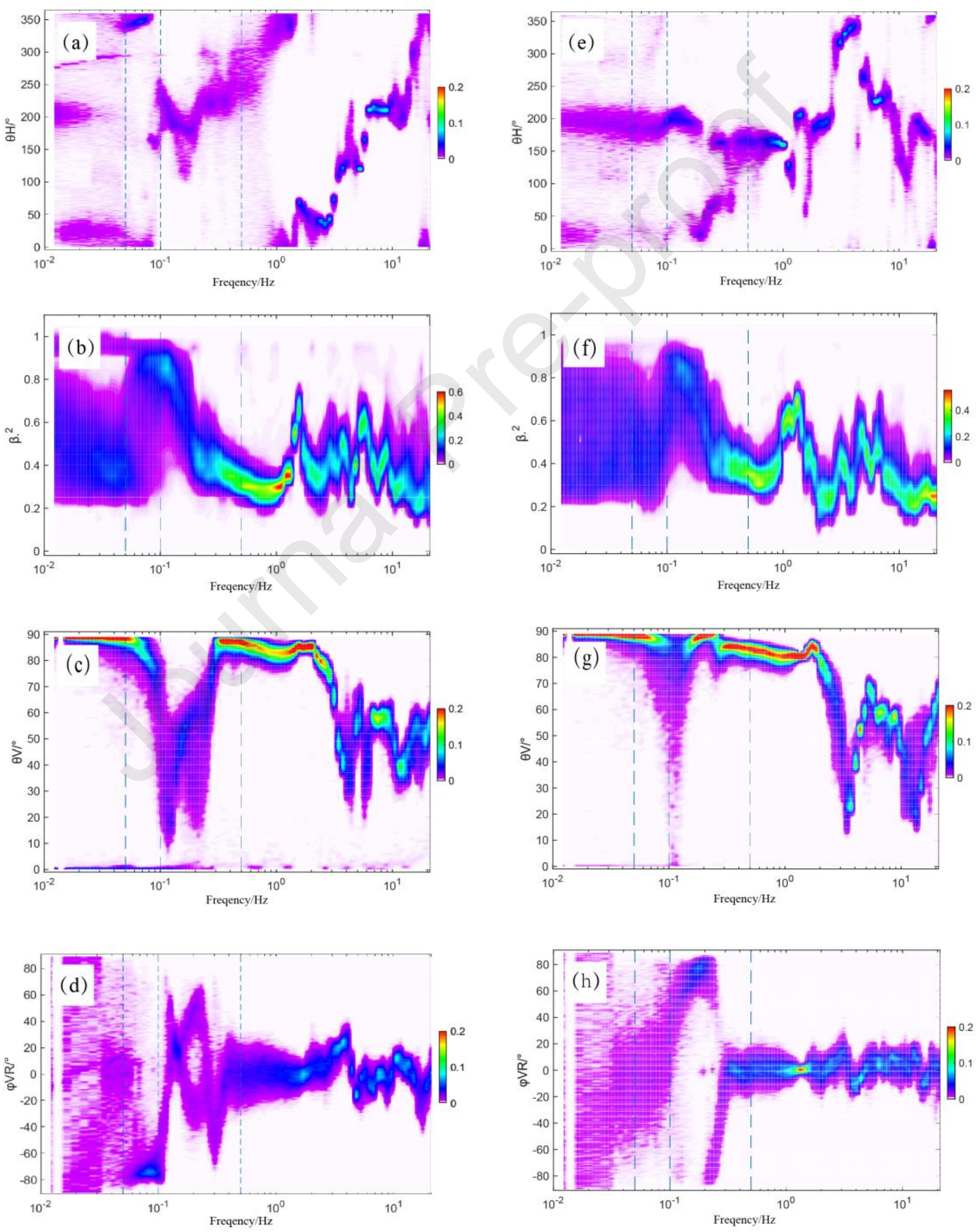

Fig. 9 Polarization analysis results for two stations: θ_H for (a) HYB05 and (e) HYB07, β^2 for (b) HYB05 and (f) HYB07, θ_V for (c) HYB05 and (g) HYB07, and φ_{VR} for (d) HYB05 and (h) HYB07

Moreover, distinct segmentation characteristics are observed near 0.2 Hz for θ_V and φ_{VR} of both stations' DF microseisms, indicating non-identical vibration properties in vertical and radial components. This suggests different energy generation mechanisms and distinct field sources between the two stations. The long-period double-frequency (LPDF) demonstrates stronger vertical vibration vectors with relatively dominant Rayleigh wave components, while the short-period double-frequency (SPDF) shows comparatively more Love wave components. These characteristics resemble observations from land-based permanent stations, confirming the reliability of at least two persistent field sources for DF microseisms in eastern China. The LPDF microseisms are more likely generated through wave-seafloor interactions in open coastal waters (Xiao and Huang, 2015; Xiao et al., 2018). However, the higher β^2 observed at offshore platforms compared to land stations may reflect non-negligible direct impacts from marine hurricanes/storm activities and corresponding platform responses.

5. Conclusions

This study adopts frequency-domain polarization analysis to investigate the ambient seismic noise characteristics (energy intensity, wavefield composition, and polarization properties) using continuous waveform data from seismometers deployed on offshore wind platforms. Complementary finite element modeling is employed to quantitatively assess platform structural responses to ambient noise excitation. The main conclusions are as follows:

(1) The average noise power at offshore platform stations ranges around -91 dB within the 1-20 Hz frequency band. Distinct SF energy is observed in the microseismic band, while the DF band exhibits clear segmentation near 0.2 Hz. This feature is consistent with that observed from island and coastal stations. Horizontal components show higher energy than vertical components, likely due to lateral wave/current forces amplifying platform vibrations directionally.

(2) Compared to land stations, offshore platforms demonstrate the noise amplification in the whole frequency range. Notably, the peak floor amplification ratios peaks between 1.2 Hz and 1.6 Hz with corresponding values ranging from 6.6 to 7.7. This can be attributed to the excitation frequency being close to the first three modal frequencies of the offshore structure, thereby causing the resonance of the structure. This can support the observed peak amplitudes in the intensity of ambient seismic noise within the range of 1~2 Hz.

(3) The continuous recording data from offshore engineering platform monitoring stations can be utilized for studying the properties of microseismic wavefields. Within the microseismic frequency band (20s-0.5Hz), the azimuth of the polarization principal axis of noise is predominantly concentrated around 200°. The low-frequency components (<0.05 Hz) exhibit a scattered distribution of β^2 ranging between 0.2 and 1. This indicates negligible kinematic differences between vertical and tangential motions of SF

microseisms, where the principal eigenvector does not represent pure Rayleigh waves but rather a hybrid composition of Rayleigh, Love, and body waves. For the high-frequency band (>1 Hz), the polarization degree exhibits perturbed variations within the 0.2–0.6 range as frequency increases, with β_2 values systematically higher than those observed at onshore stations..

Due to the high noise levels, offshore platforms might not be ideal locations for seismic observations. This study employs finite element modeling to quantitatively analyze the amplification effects of platform structures on ambient seismic noise, providing important theoretical references for subsequently improving the signal-to-noise ratio of observational data. Meanwhile, these monitoring data can be further utilized for safety assessments of the offshore structure in the future.

Acknowledgements

This research was jointly supported by the Spark Program Project of the China Earthquake Administration (XH23015A), the Industry Foresight and Key Core Technology Project of the Jiangsu Province Key Research and Development Program (BE2023082), the Director Fund Project of the Administration of Jiangsu Earthquake (202401), and the National Natural Science Foundation of China (52378345). We thank two anonymous reviewers, the associate editor and deputy editor-in-chief for their value comments during the review process.

6. References

Ajamy, A.., Asgarian, B.., Ventura, C..Zolfaghari, M., 2018. Seismic fragility analysis of jacket type offshore platforms considering soil-pile-structure interaction. Engineering Structures, 174: 198-211.

American Society of Civil Engineers, ASCE 7–16: Minimum Design Loads for Buildings and Other Structures, 2016. Reston, Virginia

Baba, S.., Araki, E.., Yokobiki, T.., Kawamata, K.., Uchiyama, K..Yoshizuka, T., 2024. Seismic observation using distributed acoustic sensing around the Tsugaru Strait at the Japan and Kuril Trenches, northeastern Japan. Earth Planets and Space, 76(1).

Bromirski, P.D.., Duennebier, F.K..Stephen, R.A., 2005. Mid-ocean microseisms. Geochemistry, Geophysics, Geosystems, 6(4).

Bromirski, P.D.., Stephen, R.A..Gerstoft, P., 2013. Are deep-ocean-generated surface-wave microseisms observed on land? Journal of Geophysical Research: Solid Earth, 118(7): 3610-3629.

Chen, G.., Qu, F.., Li, P.., Liu, Xiao., 2016. Numerical study of wave height seasonality in the Yellow Sea, Marine Sciences, 40(11): 155-168.

Chen, W., Luo, Z., Zheng, Y., Xu, L., & Huang, L. (2025). Seismic response analysis of liquefiable seabed sites: Effects of seawater-seabed interaction and bidirectional seismic motion. Ocean Engineering, 324, 120717.

Chen, Y.., Gao, L.., Zhao, F,. 2007. A method to enhance the signal/noise ratio of three-component seismic data based on the polarization analysis in frequency domain. Progress in Geophysics, 2007, 22(1): 255-261.

Flinn, E.A., 1965. Confidence regions and error determinations for seismic event location. Reviews of Geophysics, 3(1): 157-185.

GB 50011-2010. Code for Seismic Design of Buildings. Beijing: China Architecture and Building Press; 2010. (In Chinese)

Gong, J.., Sun, Y.., Zheng, J., 2023. Construction and Efficiency Analysis of Jiangsu Marine Seismic Stations. Journal of Disaster Prevention and Mitigation Engineering, 43(03):614-625.

Hasselmann, K., 1963. A statistical analysis of the generation of microseisms. Reviews of Geophysics, 1(2): 177-210.

Ito, A.., Yamamoto, Y.., Hino, R.., Suetsugu, D.., Sugioka, H.., Nakano, M.., Obana, K.., Nakahigashi, K..Shinohara, M., 2017. Tomographic image of crust and upper mantle off the Boso Peninsula using data from an ocean-bottom seismograph array. Earth Planets and Space, 69.

Jepsen, D..Kennett, B., 1990. Three-component analysis of regional seismograms. Bulletin of the Seismological Society of America, 80(6B): 2032-2052.

Jurkevics, A., 1988. Polarization analysis of three-component array data. Bulletin of the Seismological Society of America, 78(5): 1725–1743.

Koper, K.D..Burlacu, R., 2015. The fine structure of double-frequency microseisms recorded by seismometers in North America. Journal of Geophysical Research: Solid Earth, 120(3): 1677-1691.

Koper, K.D..Hawley, V.L., 2010. Frequency dependent polarization analysis of ambient seismic noise recorded at a broadband seismometer in the central United States. Earthquake Science, 23: 439-447.

Krylov, A.A.., Egorov, I.V.., Kovachev, S.A.., Ilinskiy, D.A.., Ganzha, O.Y.., Timashkevich, G.K.., Roginskiy, K.A.., Kulikov, M.E.., Novikov, M.A.., Ivanov, V.N.., Radiuk, E.A.., Rukavishnikova, D.D.., Neeshpapa, A.V.., Velichko, G.O.., Lobkovsky, L.I.., Medvedev, I.P..Semiletov, I.P., 2021. Ocean-Bottom Seismographs Based on Broadband MET Sensors: Architecture and Deployment Case Study in the Arctic. Sensors, 21(12).

Lin, C.-r.., Liao, Y.-C.., Wang, C.-c.., Kuo, B.-Y.., Chen, H.-H.., Jang, J.-p.., Chen, P.-c.., Chang, H.-k.., Lin, F.-S..Chang, K.-H., 2024. Development and evaluations of the broadband ocean bottom seismometer (Yardbird-BB OBS) in Taiwan. Terrestrial, Atmospheric and Oceanic Sciences, 35(1): 4.

Lin, J.., Yang, W.., Chen, Meng.., Wu, Renhao.., Ge Hongkui., 2012. The application of polarization analysis in seismic signal detection. Earthquake Research In China, 28(2): 133-143.

Miche, A., 1944. Mouvements ondulatoires de la mer en profondeur constante ou décroissante. Ann. Ponts Chaussees, 25: 369-406.

Park, J.., Vernon III, F.L..Lindberg, C.R., 1987. Frequency dependent polarization analysis of high-frequency seismograms. Journal of Geophysical Research: Solid Earth, 92(B12): 12664-12674.

Peterson, J.R., 1993. Observations and modeling of seismic background noise. 2331-1258, US Geological Survey.

Samson, J., 1983. Pure states, polarized waves, and principal components in the spectra of multiple, geophysical time-series. Geophysical Journal International, 72(3): 647-664.

Shinohara, M.., Yamada, T.., Akuhara, T.., Mochizuki, K..Sakai, S., 2022. Performance of Seismic Observation by Distributed Acoustic Sensing Technology Using a Seafloor Cable Off Sanriku, Japan. Frontiers in Marine Science, 9.

Stephen, R., 2003. Workshop on Seismo-Acoustics Applications in Marine Geology and Geophysics. National Science Foundation.

Sun, T.., Xue, M.., Le, K.P.., Zhang, Y..Xu, H., 2013. Signatures of ocean storms on seismic records in South China Sea and East China Sea. Marine Geophysical Research, 34(3-4): 431-448.

Sun, Y.., He, Y.., Zheng, J.., Wang, J.. 2022. A Preliminary Investigation of an M3.8 Earthquake in the South Yellow Sea Recorded by an Experimental Offshore Wind Power Platform based Seismic Station . Journal of Disaster Prevention and Mitigation Engineering,(6):1351-1353

Takagi, R.., Nishida, K.., Maeda, T..Obara, K., 2018. Ambient seismic noise wavefield in Japan characterized by

polarization analysis of Hi-net records. Geophysical Journal International, 215(3): 1682-1699.
Tanimoto, T..Prindle, K., 2007. Surface wave analysis with beamforming. Earth, planets and space, 59: 453-458.
Tsai, V.C., 2011. Understanding the amplitudes of noise correlation measurements. Journal of Geophysical Research: Solid Earth, 116(B9).
Viana P. B., Kiwamu N., Bogdan E., Ryota T.; 2025.Ocean Microseisms Recorded by the Cuban Seismic Network: Time Variation, Spectral Features, and Source Directionality Characteristics. Seismological Research Letters;; 96 (2A): 758–771
Wagner, G.S..Owens, T.J., 1996. Signal detection using multi-channel seismic data. Bulletin of the Seismological Society of America, 86(1A): 221-231.
WANG Jun, ZHENG DingChang, ZHANG JinChuan, ZHAN XiaoYan, Qian Ting. 2020. Seismic velocity changes in the epicentral region of the 2013 Lushan earthquake measured from ambient seismic noise. Chinese Journal of Geophysics (in Chinese), 63(2): 517-531
WANG Jun, ZHENG XiuFen, LIU HongGui, YANG DaKe, ZHENG DingChang, ZHENG JiangRong, ZHAN XiaoYan, SUN YeJun, DU Hang. 2022. Characteristics and location of non-random persistent microseismic ambient noise sources in eastern China. Chinese Journal of Geophysics (in Chinese), 65(5): 1660-1674
Webb, S.C., 1998. Broadband seismology and noise under the ocean. Reviews of Geophysics, 36(1): 105-142.
Xiao, H.., Xue, M.., Pan, M..Gao, J., 2018. Characteristics of microseisms in South China. Bulletin of the Seismological Society of America, 108(5A): 2713-2723.
Xiao, H..Huang, W., 2015. Three-dimensional numerical modeling of solitary wave breaking and force on a cylinder pile in a coastal surf zone. Journal of Engineering Mechanics, 141(8): A4014001.
Xu, L. Y., Huang, J. T., Liu, L., Song, C. X., Zhou, Z. L., Li, Z. Y., Cai, F, & Chen, G. X. (2025a). Offshore wind turbine monopiles under real wind and wave conditions: Considering cyclic softening of clays. Ocean Engineering, 322, 120449. https://doi.org/10.1016/j.oceaneng.2025.120449
Xu, L. Y., Xi, J. P., Jiang, J. W., Cai, F., Sun, Y. J., & Chen, G. X. (2025b). Seismic fragility analysis of shield tunnels in liquefiable layered deposits. Soil Dynamics and Earthquake Engineering, 191, 109246. https://doi.org/10.1016/j.soildyn.2025.109246
Xu, L. Y., Yuan, Z. H., Peng, X. B., Chen, W. Y., Cai, F., Zhou, Y. G., & Chen, G. X. (2025c). Seismic response analysis of offshore wind turbines supported by monopiles on gently sloping sandy seabed. Ocean Engineering, 323, 120599.
YE, S.-h..XIN, L.-l., 2024. Settlement and bearing capacity of single pile based on shear characteristics of pile-soil interface. Rock and Soil Mechanics, 45(5): 7.
ZHU Feng, YANG Chi, HE Yicheng, et al. Preliminary discussion on the earthquake early warning network of Jiangsu Province[J]. Seismological and Geomagnetic Observation and Research, 2023, 44(5): 52-58.
Zou, X.., Yang, W.., Liu, P..Wang, M., 2023. Floor acceleration amplification and response spectra of reinforced concrete frame structure based on shaking table tests and numerical study. Archives of Civil and Mechanical Engineering, 23(3): 156.

Characteristics of Ambient Seismic Noise Recorded at Offshore Wind Turbine Platform Monitoring Stations

Jun Wang , Jiang-rong Zheng， Ye-jun Sun， Ling-yu Xu, Yi-cheng He , Jie Gong , Chen Wang, Xiao-yan Zhan, Yu-jie Wan , Wen-jie Ren

1、Jun Wang, Professor, Earthquake Administration of Jiangsu Province, Nanjing 210014, China.
Email: wangjun1099@qq.com, Phone: 13951702501.

2、Jiang-rong Zheng， Professorr,Earthquake Administration of Jiangsu Province, Nanjing 210014, China.
Email: jsdzjzjr@126.com.

3、Ye-jun Sun，Professor,Earthquake Administration of Jiangsu Province, Nanjing 210014, China.
Email: syj_4116@126.com.

4、**Ling-yu Xu，** Professor Institute of Geotechnical Engineering, Nanjing Tech University, Nanjing 210009, China.
Email: lyxu@njtech.edu.cn

5、**Yi-cheng He，** Associate professor,Earthquake Administration of Jiangsu Province, Nanjing 210014, China.
Email: hyckevin@mail.ustc.edu.cn

6、Jie Gong， Associate professor, Earthquake Administration of Jiangsu Province, Nanjing 210014, China. Email: 498602259@qq.com

7、Chen Wang， Engineer, Earthquake Administration of Jiangsu Province, Nanjing 210014, China.
Email:372766770@qq.com

8、Xiao-yan Zhan， Associate professor, Earthquake Administration of Jiangsu Province, Nanjing 210014, China. Email: 43493270@qq.com

9、Yu-jie Wan， Engineer, Earthquake Administration of Qinghai Province, Xining 810000, China.
Email:376633212@qq.com

10、**Wen-jie Ren，**PhD candidate, Institute of Geotechnical Engineering, Nanjing Tech University, Nanjing 210009, China.
Email:renwenjie@njtech.edu.cn

Corresponding author: Jun Wang, wangjun1099@qq.com

Table 2 Detailed parameters of two equipment used for marine seismic observation

Serial Number	Equipment	Seismometer Sensitivity	Data Logger Conversion Factor	Sampling Rate	Frequency Bandwidth
1	GL-PCS60	1000 V/m/s	74.5nV/count	100Hz	60s-50Hz
2	GL-PS2	1000 V/m/s	74.5nV/count	100Hz	2s-50Hz

Declaration of interests

The authors declare that they have no known competing financial interests or personal relationships that could have appeared to influence the work reported in this paper.